Mechanics Research Communications 129 (2023) 104088

Contents lists available at ScienceDirect

Mechanics Research Communications

journal homepage: www.elsevier.com/locate/mechrescom

Discontinuous bifurcation of FRCC with zero-thickness interface modeling

Antonio Caggiano [a,*], Sonia M. Vrech [b], Guillermo J. Etse [b,c]

[a] DICCA, Dept. of Civil, Chemical and Environmental Engineering, University of Genova, Via Montallegro 1, Genova 16145, Italy
[b] CEMNCI, Center for Numerical and Computational Methods in Engineering, National University of Tucuman, Argentina
[c] LMNI, Laboratory of Numerical Methods in Engineering, Universidad de Buenos Aires, CONICET, Buenos Aires, Argentina

ARTICLE INFO

Keywords:
Discontinuous-based approach
Fracture
Cement-based composites
Fibers
Cracking indicator
Mesoscale

ABSTRACT

In this work, firstly a fracture-based interface constitutive theory, aimed at simulating the cracking mechanisms of Fiber Reinforced Cementitious Composites (FRCCs), is presented. The discontinuous formulation assumes a hyperbolic maximum strength criterion in terms of normal and shear joint stresses. The latter are evaluated on each crack front to simulate the failure behavior of plain and FRCC systems. A non-associated plastic flow rule, in conjunction with a post-cracking softening law, is defined to complete the modeling approach. On the other hand, the use of the most-classical Mixture Theory is followed for taking into account the actions of fibers in concrete matrix. The bridging mechanisms between fibers and active cracks are defined in terms of fiber-to-concrete bond–slip rule and dowel effects. Secondly, a normalized Cracking Indicator (CI) for discrete crack is proposed in the spirit of Hill's indicator for loss of stability of inelastic continua, to effectively evaluate the most critical direction for further loading in terms of the resulting energy release and crack opening, while accounting for the fiber direction and content. After presenting the constitutive theory and, particularly, the novel concept of the CI, numerical analyses at constitutive level are performed to evaluate the evolution of the fracture energy, post-peak strength, and critical cracking directions under variable fiber contents. Different load scenarios are evaluated, and the numerical predictions are compared with experimental data.

1. Introduction

Cement-based composites like concrete are the most widely used construction materials. A great part of the existing built stock, and the majority of worldwide infrastructures, are prevalently made of reinforced concrete. However, they are characterized by a quite low tensile strength, together with a very fragile response. The addition of short reinforcements, like fibers, in the cementitious matrix can basically overcome these deficiencies [1]. FRCCs may offer less brittleness and sometimes behaving with a quasi-ductile response, even under tensile loading [2]. By adding high fiber percentages, strain-hardening responses with multiple cracks, and large energy absorption prior failure, can be achieved under tension and bending [3]. In this regard, fiber types, materials, and geometric details [4] (i.e., diameters, lengths, and aspect ratios) can have a huge influence on the resulting bridging mechanisms, which drive the type of fracture mechanisms of FRCC. Experimental studies demonstrated that the random dispersion of short fibers can enhance the response of the composites in the post-cracking regime, with several advantages [5,6]: i.e., improved tensile/shear strengths, better post-cracking ductility, higher fracture energy, etc.

The incorporation of fibers and their design, also in partial substitution of classical rebars, grew up considerably in the last thirty years. Most popular designing EU and international guidelines/codes including them are, for example, the Austrian guidelines [7], the French recommendations [8], the German ones [9], the Italian rules [10], the Spanish codes [11], the Sweden codes [12], the Swiss recommendations [13] and those provided by the RILEM Committee [14] together with the worldwide adopted fib Model-Code [15]. The US standards for FRCC to be mentioned are the [16,17].

Theoretical constitutive models and numerical tools are needed for describing and predicting the non-homogeneous FRCC cracking onset and propagation. In this sense, the simulation of cracking processes in solids and structures is still an open issue and of great interest in computational mechanics. Traditionally approaches are those based in classical continuum (namely, Smeared Crack Approaches — SCAs) in which the failure and cracked zone is considered to be distributed along a certain region of the solid [18,19]. Clear advantage of SCA is its simpleness to be implemented in continuous Finite Element (FE) programs (even commercial ones). However, the main drawback of SCA is the associated strong FE size dependency of the localization band, and, consequently, the objectivity loss of their results [20]. Thus,

* Corresponding author.
E-mail address: antonio.caggiano@unige.it (A. Caggiano).

https://doi.org/10.1016/j.mechrescom.2023.104088
Received 12 September 2022; Received in revised form 16 January 2023; Accepted 2 March 2023
Available online 5 March 2023

opportune regularization procedures need to be considered to avoid these shortcomings of SCA [21,22]. On the other hand, Discrete Crack Approaches (DCAs), which incorporate strains and/or displacement jumps/discontinuities, can represent an alternative approach to describe cracks and related evolution mechanisms at the fracture front of the failure process. Many options can be undertaken for concrete and FRCC in this field, i.e.: zero-thickness interfaces [23], lattice and particle procedures [24], discontinuous VEM [25], X-FEM [26] and E-FEM [27]. Among these techniques, the main advantages of using zero-thickness interfaces are (i) the remeshing is not needed, (ii) the automatic regularization of the solution, since the discontinuities in the displacement field is directly account at joints (cracks) level, thus, there is no need to require localized deformation capabilities of the continuum elements and (iii) their easy implementation in FEM codes.

For both diffuse and discrete approaches, localized failure modes must be analyzed to identify the cracking onset. In the framework of the SCA, localized failure modes are related to discontinuous bifurcations of the equilibrium path which leads to the lost of ellipticity of the equations, that govern the static equilibrium problem. The localized deformation field exhibits a plane of discontinuity that can be identified by means of the eigenvalue problem of the acoustic (also known as localization) tensor [28]. Analytical solutions for the discontinuous bifurcation condition, based on original works by Hadamard [29], Thomas [30] and Hill [31], can conduce to the so-called macroscopic localization condition. In this context, the derivation of the discontinuous bifurcation condition for the case of the SCA microplane theory for FRCC have been obtained by the authors of this work (see [32]), including the variation of fiber contents and directions influence. The key contribution of the paper deals with proposing a novel normalized cracking indicator (CI) for FRCC interface constitutive models based on the mixture theory. The proposed CI follows the concept of the normalized indicator for diffuse failure by Hill's condition of stability, typically built up for continuous-based procedures. This CI provides objective useful information on the critical directions for further loading regarding the overall energy release due to the degradation mechanisms in the different mixture components, while at the same time it assesses the effect of the fiber content and its direction on the expectable energy release for the whole spectrum of possible loading directions.

After this general introduction section, the paper is structured as follows. Section 2 summarizes the constitutive formulation of the zero-thickness interface model for failure behavior of FRCC. Section 3 discusses the theoretical background of strain localization problems: the discontinuous bifurcation condition for SCA and later the concept of failure indicators for the case of zero-thickness interface FRCC models, proposing a normalized scalar for DCA. Then, numerical simulations compared against available experimental data are presented in Section 4 with the aim to verify the soundness and capabilities of the methodology. Section 5 presents the failure performance and the CI results for mixed modes of fracture and variable fiber contents in terms of critical failure directions. Finally, some concluding remarks are made in Section 6.

2. Zero-thickness interface model for FRCC

The present constitutive model for FRCC was inspired to a discrete-crack approach (see [33]) adding the combination of the fibers, mechanically described as beam elements crossing the interfaces. It accounts for three internal constitutive formulations: i. The fracture energy-based plasticity formulation for plain mortar/concrete joints, as summarized in Section 2.1; ii. Fiber bond–slip developed in the axial direction of fibers. Pull-out mechanisms of fibers crossing cracks are formulated through a 1D elasto-plastic model; iii. Dowel action (only for metallic fibers) based on elastic beam foundation theory to get the transversal force–displacement relationship. Both modeling as of points ii. and iii. are detailed in Section 2.2.

Table 1
Overview of the interface constitutive model for concrete.

	Fracture-based energy interface model
Constitutive relationships	$\dot{\mathbf{u}} = \dot{\mathbf{u}}^{el} + \dot{\mathbf{u}}^{cr}$ $\dot{\mathbf{u}}^{el} = \mathbf{C}^{-1}\cdot\dot{\mathbf{t}}$ $\dot{\mathbf{t}} = \mathbf{C}\cdot\left(\dot{\mathbf{u}} - \dot{\mathbf{u}}^{cr}\right)$
Yield condition	$f(\mathbf{t},\kappa) = \sigma_T^2 - (c - \sigma_N \tan\phi)^2 + (c - \chi\tan\phi)^2 \le 0$
Flow rule	$\dot{\mathbf{u}}^{cr} = \dot{\lambda}\mathbf{m}$ $\mathbf{m} = \mathbf{A}\cdot\mathbf{n}$
Cracking work-evolution	$\dot{\kappa} = \dot{w}_{cr}$ $\dot{w}_{cr} = \sigma_N\cdot\dot{u}^{cr} + \sigma_T\cdot\dot{v}^{cr}$ $\quad \sigma_N \ge 0$ $\dot{w}_{cr} = \left[\sigma_T - \lvert\sigma_N\rvert tan(\phi)\right]\dot{v}^{cr}$ $\quad \sigma_N < 0$
Evolution law of internal parameters	$p_i = \left(1-\left(1-r_{pi}\right)S[\xi_{p_i}(\kappa)]\right)p_{0i}$
Kuhn - Tucker loading/unloading and consistency conditions	$\dot{\lambda} \ge 0,\quad f \le 0,\quad \dot{\lambda} f = 0$ **Kuhn-Tucker** $\dot{f} = 0$ **Consistency**

2.1. Fracture energy-based interface model for concrete

This section describes the fracture-based constitutive model for cement-based materials implemented into zero-thickness interfaces and based on a hyperbolic yield surface and a non-associated flow rule. Table 1 gives its the main features whilst full details are available in previous contributions by the authors (see for example [23,34]). In Table 1, $\mathbf{C}$ represents the uncoupled joint elastic stiffness matrix, $\dot{\mathbf{u}}^{el}$ and $\dot{\mathbf{u}}^{cr}$ the elastic and cracking displacement rate vectors, respectively, and $\mathbf{t} = [\sigma_N, \sigma_\tau]^t$ is the joint stress vector. $f(\mathbf{t},\kappa)$ is the hyperbolic yield condition, based on three main parameters: the tensile strength χ, the cohesion c and the friction angle ϕ. The cracking displacement evolution $\dot{\mathbf{u}}^{cr} = [\dot{u}^{cr}, \dot{v}^{cr}]^t$ is evaluated by means of a non-associated flow rule, which defines the inelastic direction $\mathbf{m}$ through the transformation operator A, that affects the associated normal flow derivative, $\mathbf{n} = \partial f/\partial\mathbf{t}$. $\dot{\lambda}$ is the non-negative cracking multiplier, achieved by means of the Kuhn–Tucker and consistency conditions. The fracture work rate $\dot{w}_{cr}$ is adopted as the internal variable which affects the softening evolution laws and, consequently, the loading surfaces. Unified decay functions are considered for each the three internal parameters of the yield function, χ, c and $\tan(\phi)$, represented alternatively by p_i; where p_{0i} symbolized their initial values, $r_p p_{0i}$ the residual ones and $S[\xi_{p_i}]$ the scaling functions, being ξ_{p_i} the ratio between the current work spent and the available fracture energy (i.e., in mode I and/or II).

2.2. Fiber mechanisms: Pull-out and dowel effects

FRCC can be modeled at a meso-scale standpoint by explicitly considering the effect of fibers crossing active cracks. If the fracture process is modeled through interfaces and DCA, the transferred stresses between cracks due to fibers bridging effects can be considered via 1D modeling tools, smeared with the well-known Mixed Theory [23]. The number of fibers crossing the interface is calculated as a function of the volume fraction and their geometric characteristics. Then, their mechanical contributions are considered via two plasticity-based constitutive models: for the bond–slip behavior in the axial fibers direction and for the dowel mechanism in the transversal one.

On the one hand, a one-dimensional plasticity model accounting for a stress–strain response is employed to describe the fiber bond–slip response. The main functions of the adopted bi-linear stress–strain rule ($\sigma_f - \varepsilon_N$) are summarized in Table 2. It is based on the additive decomposition of the total strain rate $\dot{\varepsilon}_N$, into elastic and plastic components, $\dot{\varepsilon}_N^{el}$ and $\dot{\varepsilon}_N^{pl}$, respectively. $\dot{\sigma}_f$ is the total normal stress rate while E_f is the uniaxial elastic modulus which considers both the uniaxial response of the fiber and the bond–slip effect of the short reinforcement in concrete substrate. f_f is the yield condition, being $\sigma_{y,f}$ the initial yield stress and Q_f the dissipative stress in post-elastic regime. Its evolution law is defined in terms of the incremental

Table 2
Bond–slip constitutive model for fibers crossing cracks.

	1D bond-slip model
Constitutive relationships	$\dot{\varepsilon}_N = \dot{\varepsilon}_N^{el} + \dot{\varepsilon}_N^{pl}$ $\dot{\sigma}_f = E_f(\dot{\varepsilon}_N - \dot{\varepsilon}_N^{pl})$
Yield condition	$f_f = \lvert\sigma_f\rvert - (\sigma_{y,f} + Q_f) \le 0$
Flow rule	$\dot{\varepsilon}_N^{pl} = \dot{\lambda}_f \partial f_f / \partial \sigma_f = \dot{\lambda}_f sign[\sigma_f]$
Internal evolution law	$\dot{Q}_f = \dot{\lambda}_f H_f$
Kuhn - Tucker loading/unloading and consistency conditions	$\dot{\lambda}_f \ge 0, f_f(\sigma_f, Q_f) \le 0, \dot{\lambda}_f f_f(\sigma_f, Q_f) = 0$ $\dot{f}_f(\sigma_f, Q_f) = 0$

Table 3
Dowel constitutive model for fibers crossing cracks.

	1D dowel model
Constitutive relationships	$\dot{\gamma}_T = \dot{\gamma}_T^{el} + \dot{\gamma}_T^{pl}$ $\dot{\tau}_f = G_f(\dot{\gamma}_T - \dot{\gamma}_T^{pl})$
Yield condition	$g_f = \lvert\tau_f\rvert - (\tau_{y,f} + R_f) \le 0$
Flow rule	$\dot{\gamma}_T^{pl} = \dot{\lambda}_f \partial g_f / \partial \tau_f = \dot{\lambda}_f sign[\tau_f]$
Internal evolution law	$\dot{R}_f = \dot{\lambda}_f K_f$
Kuhn - Tucker loading/unloading and consistency conditions	$\dot{\lambda}_f \ge 0, g_f(\tau_f, R_f) \le 0, \dot{\lambda}_f g_f(\tau_f, R_f) = 0$ $\dot{g}_f(\tau_f, R_f) = 0$

plastic multiplier $\dot{\lambda}_f$ and the softening normal module H_f. On the other hand, a numerical sub-model for the dowel mechanism has been also accounted by defining both stiffness and strength of a generic fiber embedded in the concrete matrix and subjected to a possible transverse force/displacement at the fracture level. The well-known Winkler beam theory is used to describe the dowel force–displacement relationship, which is then transformed in terms of dowel stress vs. relative displacement, defining the equivalent shear beam stiffness. A bi-linear shear stress–strain ($\tau_f - \gamma_T$) is adopted with the complementary functions shown in Table 3. The additive decomposition of the total strain rate $\dot{\gamma}_T$, in elastic and plastic parts, $\dot{\gamma}_T^{el}$ and $\dot{\gamma}_T^{pl}$ respectively, is also adopted. $\dot{\tau}_f$ is the total shear stress rate while G_f is the elastic modulus which considers the transversal Winkler response of the fibers. g_f is the yield condition, being $\tau_{y,f}$ the initial yield stress and R_f the dissipative stress in post-elastic regime. Its evolution law is defined in terms of the incremental plastic multiplier $\dot{\lambda}_f$ and the softening shear module K_f. The complete derivation of these two models and theirs validations against experimental data are proposed in previous works published by the authors, see [35].

3. Failure indicators for continuum models and discontinuous-based analysis

This section summarizes the failure indicators for both, SCA and DCA, that allow the calculation of the failure onset conditions and the critical post-cracking directions for variable load states and fiber contents.

3.1. Failure indicator for SCA

Analytical solutions for the discontinuous bifurcation condition regarding SCA are based on original works by Hadamard (1903) [29], Thomas (1961) [30] and Hill (1962) [31]. They conduce to the macroscopic localization condition, such as

$$\det(\boldsymbol{Q}^{ep}) = 0\,, \tag{1}$$

being $\boldsymbol{Q}^{ep}$ the elasto-plastic acoustic or localization tensor, defined as

$$\boldsymbol{Q}^{ep} = \boldsymbol{N}_c \cdot \boldsymbol{E}_c^{ep} \cdot \boldsymbol{N}_c\,, \tag{2}$$

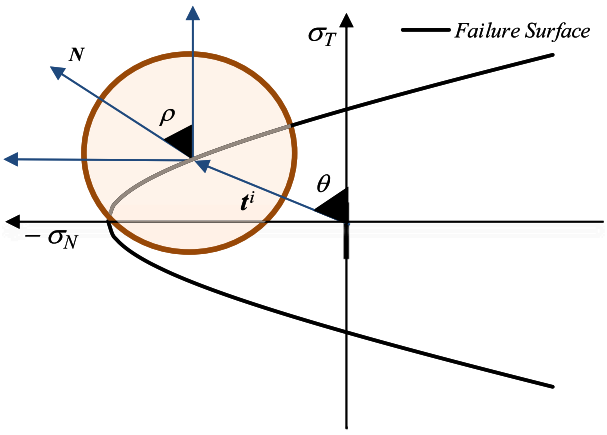

Fig. 1. Evaluation of the CI: ρ and θ-angles define the initial cracking stage and the post-cracking direction, respectively.

with $\boldsymbol{N}_c$, the normal direction to the discontinuity surface and $\boldsymbol{E}_c^{ep}$ the elasto-plastic tangent tensor of the continuum SCA model, that can be expressed in terms of the elastic one $\boldsymbol{E}_c$, as

$$\boldsymbol{E}_c^{ep} = \boldsymbol{E}_c - \frac{1}{h}\boldsymbol{E}_c : \frac{\partial Q}{\partial \boldsymbol{\sigma}} \otimes \frac{\partial F}{\partial \boldsymbol{\sigma}} : \boldsymbol{E}_c\,, \tag{3}$$

whereby the generalized plastic modulus h is defined as

$$h = \frac{\partial F}{\partial \boldsymbol{\sigma}} : \boldsymbol{E}_c : \frac{\partial Q}{\partial \boldsymbol{\sigma}} + H\,, \tag{4}$$

in terms of the derivatives of the yield function F and the plastic potential Q respect to the stress tensor $\boldsymbol{\sigma}$ and the hardening/softening variable H.

The localized failure condition of Eq. (1) leads to the analysis of the spectral properties of $\boldsymbol{Q}^{ep}$, that can be also written as

$$\boldsymbol{Q}^{ep} = \boldsymbol{Q} - \frac{1}{h}\boldsymbol{a} \otimes \boldsymbol{a}^* \quad \text{with} \quad \boldsymbol{Q} = \boldsymbol{N}_c \cdot \boldsymbol{E}_c \cdot \boldsymbol{N}_c \tag{5}$$

and the vectors $\boldsymbol{a}$ and $\boldsymbol{a}^*$ defined as

$$\boldsymbol{a} = \frac{\partial F}{\partial \boldsymbol{\sigma}} : \boldsymbol{E}_c \cdot \boldsymbol{N}_c \quad , \quad \boldsymbol{a}^* = \boldsymbol{N}_c \cdot \boldsymbol{E}_c : \frac{\partial Q}{\partial \boldsymbol{\sigma}}\,. \tag{6}$$

The smallest autovalue of $\boldsymbol{Q}^{ep}$, with respect to the metric defined by $(\boldsymbol{Q})^{-1}$, is

$$\lambda^{(1)} = 1 - \frac{\boldsymbol{a}(\boldsymbol{N}_c) \cdot \left[\boldsymbol{Q}(\boldsymbol{N}_c)\right]^{-1} \cdot \boldsymbol{a}^*(\boldsymbol{N}_c)}{h}\,. \tag{7}$$

By replacing Eqs. (4) and (6) into (7), results the localization condition such as

$$H_{cr} + \frac{\partial F}{\partial \sigma} : \boldsymbol{E}_c : \frac{\partial Q}{\partial \sigma} - \boldsymbol{a} \cdot \left[\boldsymbol{Q}(\boldsymbol{N}_c)\right]^{-1} \cdot \boldsymbol{a}^* = 0\,, \tag{8}$$

that serves as a basis for analytical and numerical evaluations of the most critical (maximum) hardening parameter $H_{cr} = \max[H(\boldsymbol{N}_c)]$ for discontinuous bifurcation and of their associated localization directions $\boldsymbol{N}_c$.

3.2. Cracking indicators for DCA

The proposed cracking indicator for DCA can be considered to be in principle similar as the one achieved for continuum-based models (SCA) as of Section 3.1.

By following the normalized indicator for diffuse failure by Hill's condition of stability, employed in SCA as in the previous section [36], it is proposed the following normalized Cracking Indicator (CI) for DCA, as for the case of zero-thickness interface models for FRCC, as

$$CI(\theta, \rho) = \frac{\boldsymbol{N}^t \cdot \boldsymbol{E}^{ep} \cdot \boldsymbol{N}}{\boldsymbol{N}^t \cdot \boldsymbol{E} \cdot \boldsymbol{N}}\,, \tag{9}$$

Table 4
Critical failure directions for SFRC.

θ	$\rho_{cr,3.0\%}$	$\rho_{cr,6.0\%}$
90°	90°	90°
75°	83.15°	85.31°
60°	76.65°	80.26°
45°	67.99°	73.77°
30°	57.17°	65.11°
15°	43.47°	52.85°

being θ the initial cracking direction angle ($\tan(\theta) = \sigma_N/\sigma_T$, as shown in Fig. 1) and $\boldsymbol{N}$ a unitary vector defining the normal of a potential cracking direction, i.e.

$$\boldsymbol{N} = [\cos(\rho), \sin(\rho)]^t \tag{10}$$

The angle ρ describe the set of all possible vectors $\boldsymbol{N}$ upon the failure criterion, as highlighted in Fig. 1, while $\boldsymbol{E}^{ep}$ represents the constitutive tangent operator, given by

$$\boldsymbol{E}^{ep} = w_{\rho_m}\boldsymbol{C}^{ep} + \sum_{f=1}^{n_f} w_{\rho_f}\left(\frac{E_f^{ep}}{l_f}\boldsymbol{n}_N \otimes \boldsymbol{n}_N + \frac{G_f^{ep}}{l_f}\boldsymbol{n}_T \otimes \boldsymbol{n}_T\right) \tag{11}$$

which depends on the weighting functions w_{ρ_m} and w_{ρ_f}, $\boldsymbol{n}_N \otimes \boldsymbol{n}_N$ and $\boldsymbol{n}_T \otimes \boldsymbol{n}_T$ identify the second order dyadic tensor constructed on the fiber direction and its orthogonal for a generic fiber with respect to the global Cartesian reference system. The tangent operators $\boldsymbol{C}^{ep}$, E_f^{ep} and G_f^{ep} are the elasto-plastic operators of the constitutive models of Section 2. Whereas n_f and l_f are the number and length of the fibers crossing the interface, respectively. Finally, $\boldsymbol{E}$ in Eq. 5 is the interface operator under elastic response, evaluated in terms of the elastic operators $\boldsymbol{C}$, E_f and G_f, similarly as Eq. (11).

The CI performance parameter can be thus computed and plotted in terms of ρ-angles (i.e., those between σ_N and σ_T stresses): i.e., $\rho = \frac{\pi}{2}$ indicates the case of pure tensile failure (namely fracture mode I), while $\rho = 0$ the direct shear with zero (confinement) pressure. For any given θ angle, a particular value for ρ (labeled as the critical one ρ_{cr}) can be numerically evaluated for which the CI parameter assumes its minimum. Under this circumstance ρ_{cr} defines the weakness direction of the considered composite FRCC interface.

4. Zero-thickness interface model performances

With the aim to demonstrate the soundness and capabilities of the proposed methodology for cementitious materials, this section proposes some applications of the zero-thickness interface constitutive model for FRCC failure analysis. First, numerical simulations against available experimental data of mixed fracture mode tests for plain concrete are shown. Then, numerical analyses of the uniaxial tensile test are carried out on both plain concrete and Steel-FRC (SFRC). Finally, critical condition for localized failure are analyzed by means of numerical analysis of the proposed CI performance. These studies allow to evaluate the sensitivity of the cracking onset and critical directions on the load state and fibers orientation.

4.1. Mixed fracture modes

To assess the predictive capability of the proposed interface constitutive model for cementitious composites under mixed-modes of fracture, the plane concrete panels by [37] are considered. These experimental tests are performed on prismatic concrete specimens of 0.07 × 0.07 m^2 cross section with a 0.015 m deep notch along their perimeter (see Fig. 2). Both normal and transverse relative displacements are imposed simultaneously to the two parts of the notched specimen with the aim to reproducing the cracking processes in concrete under mode I and II types of failure, depending on the angle between the two

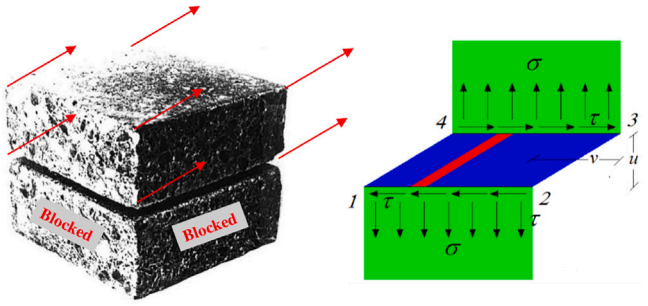

Fig. 2. Concrete prisms under mixed fracture modes by [37].

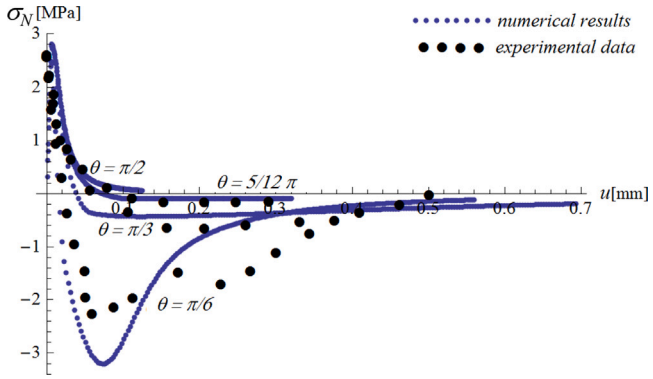

Fig. 3. Numerical predictions vs. exp. data [37]: σ_N vs. u.

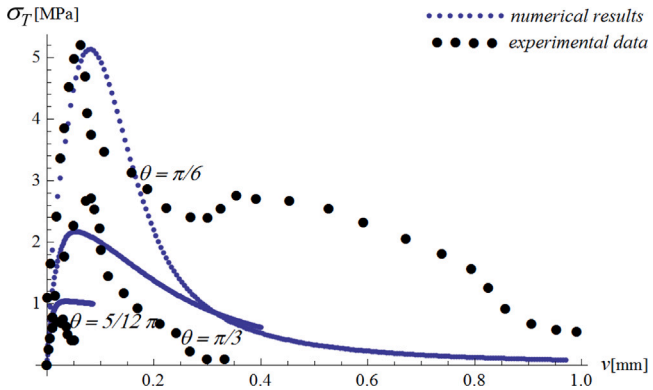

Fig. 4. Numerical predictions vs. exp. data [37]: σ_T vs. v.

displacement components. First stage of tests, normal displacements are applied until the peak strength is reached. In a second stage, tensile displacements are combined with transverse ones, on the upper part of the notched specimen, defining an θ angle ($\tan(\theta) = \sigma_N/\sigma_T$).

Four cases are evaluated, θ = 90°, 75°, 60° and 30°. The interface parameters, calibrated upon the experimental data by [37], are k_N = 500 MPa/mm, k_T = 200 MPa/mm, $\tan(\phi_0) = \tan(\beta_0) = \tan(\phi_r)$ = 0.6, χ_0 = 2.8 MPa, c_0 = 7.0 MPa, G_f^I = 0.08 N/mm, $G_f^{IIa} = 10G_f^I$, σ_{dil} = 15 MPa. The remaining parameters are considered equal to zero. For the continuum elements, the Young modulus and Poisson's ratio are E_c = 25 GPa and ν = 0.2, respectively.

The tensile stress–displacement ($\sigma_N - u$) relationship for plain concrete by [37] and the corresponding numerical predictions are shown in Fig. 3. This figure depicts the curves for θ = 90°, 75°, 60° and 30°. As it can be seen, the combined normal and shear displacements cause a more pronounced softening branch in post-peak regime. The tensile strength tends to zero more rapidly and, moreover, changes its sign

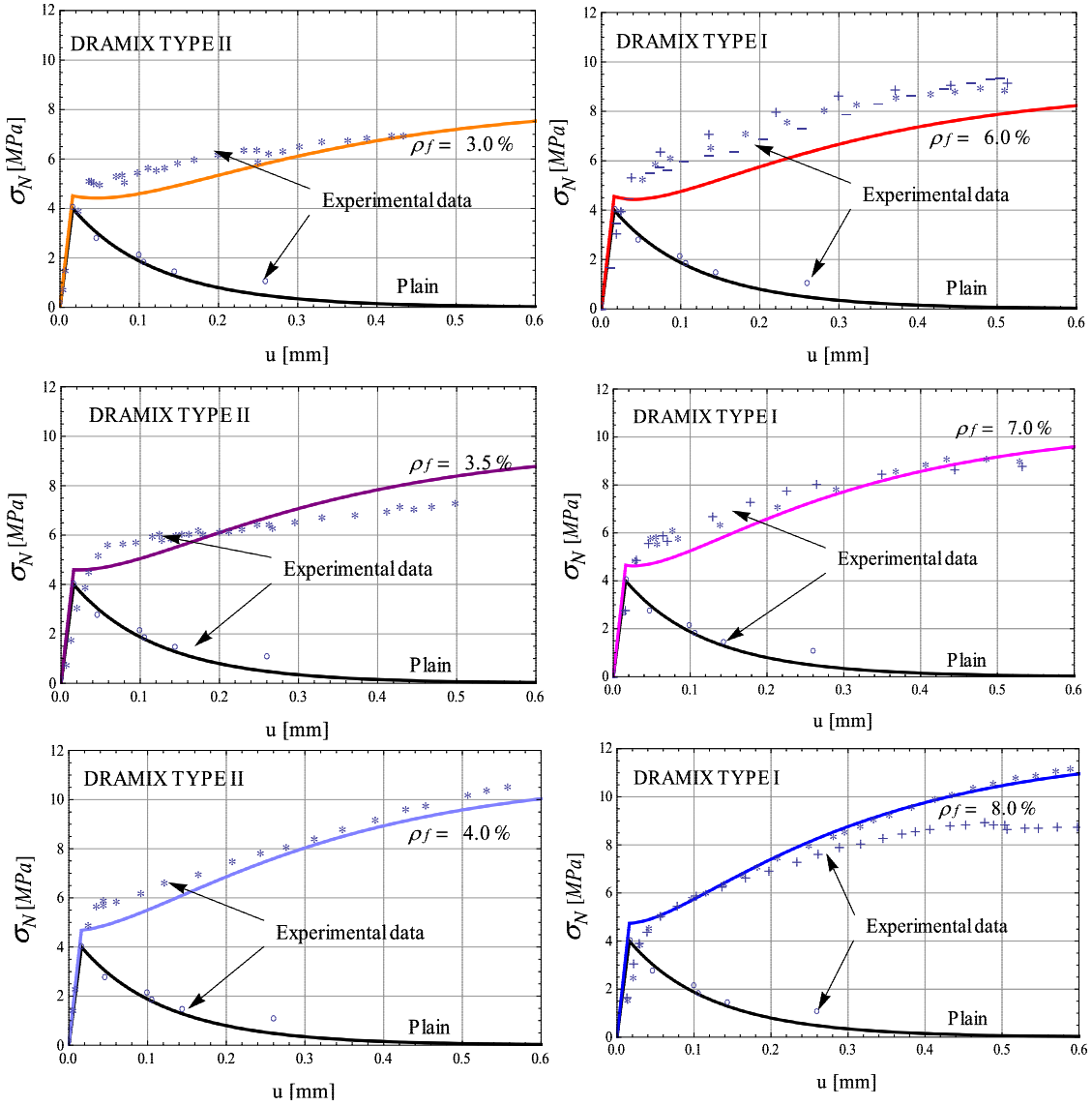

Fig. 5. Numerical predictions vs. experimental data by [38]: SFRC with "Dramix type I" and "Dramix type II" fibers.

becoming a compressive stress, due to fact that the normal dilatancy produced by the applied shear displacements, exceeds the fixed normal opening rate.

Fig. 4 compares experimental data with the numerical simulations in terms of shear stresses vs. relative transverse displacements ($\sigma_T - v$) for $\theta = 75°$, 60° and 30°. Shear strengths increase when θ decreases. It is shown a very good agreement regarding peak and residual strengths, as well as pre- and post-peak responses. The post-cracking stages are characterized by a crack-softening behavior which, as a matter of fact, is well captured through the proposed constitutive model.

4.2. Uniaxial tensile tests

The tensile tests on SFRC specimens by Li et al. [38] are considered in this section. The experimental campaign have been performed on prismatic specimens with the dimensions 500 ×100 × 20 mm^3. Two different types of steel fibers are considered namely Dramix I and II, whose fundamental common properties are: Density = 7.8 g/cm^3, Diameter = 0.5 mm, σ_y = 1.2 GPa, E = 200 GPa, while the lengths of Dramix I is 30 mm and of II is 50 mm.

The model parameters were adjusted according to the experimental data given by the authors, being the elastic properties of the rigid

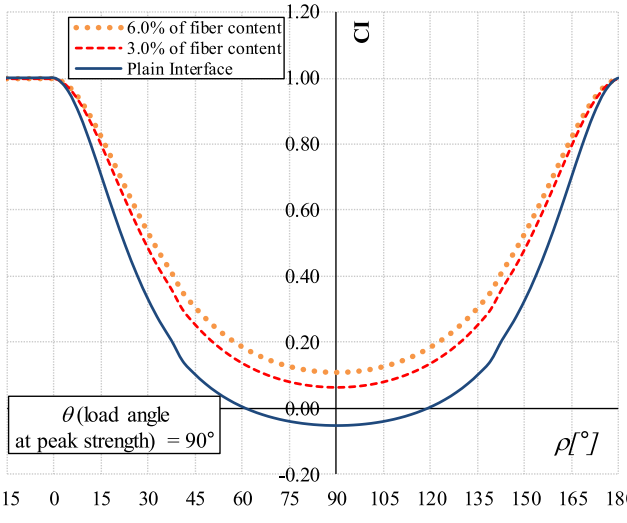

Fig. 6. CI at peak stress for $\theta = 90°$ considering plain concrete and FRCC with "Dramix I" with fiber contents of 3.0% and 6.0%.

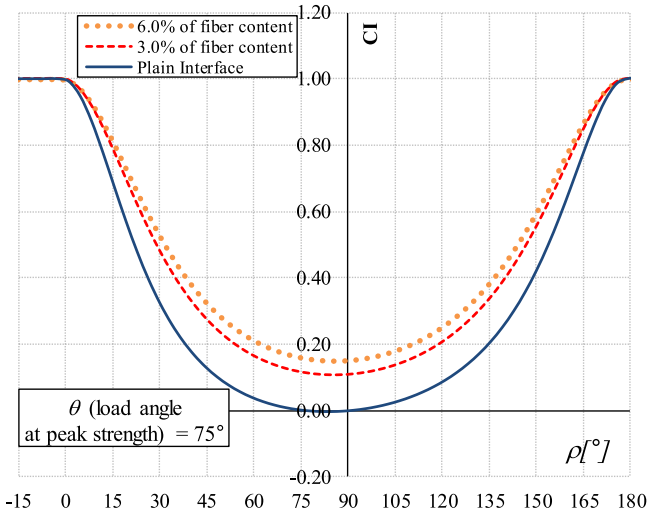

Fig. 7. CI at peak stress for $\theta = 75°$ considering plain concrete and FRCC with "Dramix I" with fiber contents of 3.0% and 6.0%.

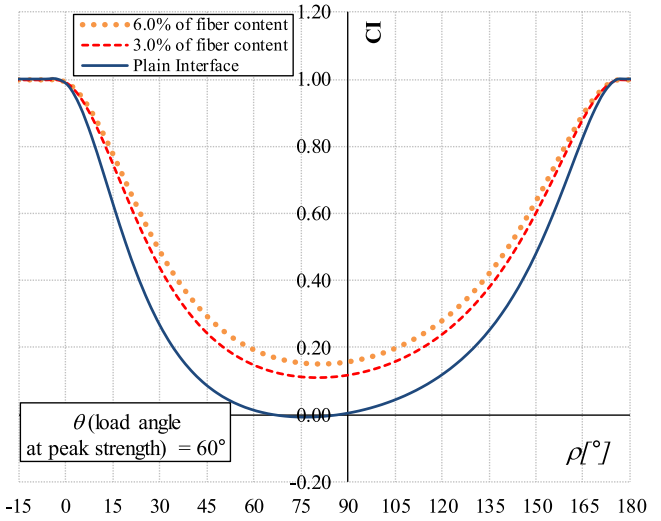

Fig. 8. CI at peak stress for $\theta = 60°$ considering plain concrete and FRCC with "Dramix I" with fiber contents of 3.0% and 6.0%.

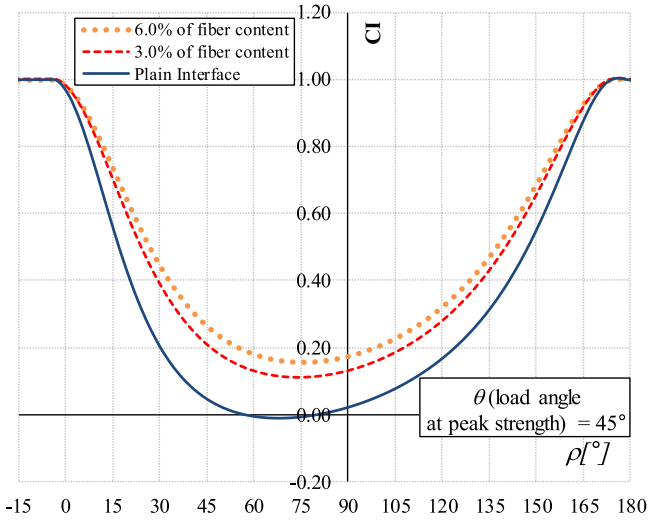

Fig. 9. CI at peak stress for $\theta = 45°$ considering plain concrete and FRCC with "Dramix I" with fiber contents of 3.0% and 6.0%.

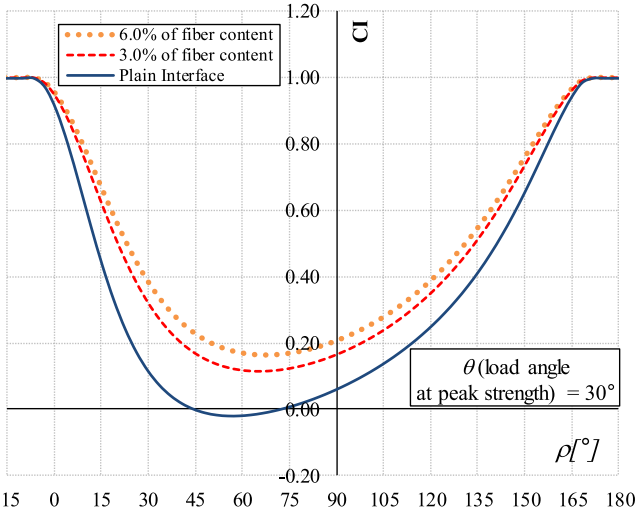

Fig. 10. CI at peak stress for $\theta = 30°$ considering plain concrete and FRCC with "Dramix I" with fiber contents of 3.0% and 6.0%.

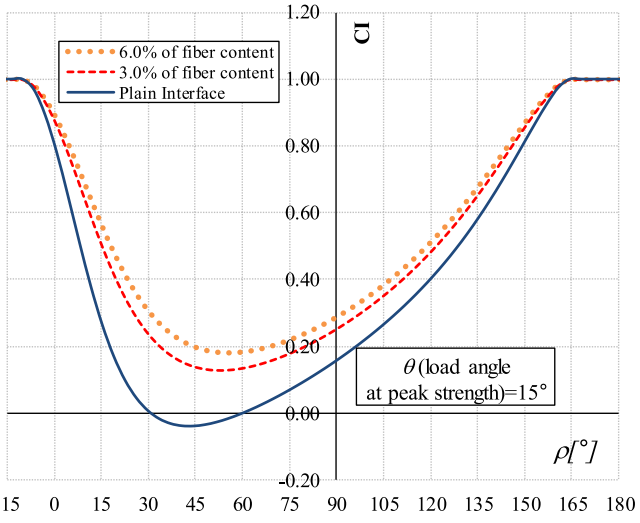

Fig. 11. CI at peak stress for $\theta = 15°$ considering plain concrete and FRCC with "Dramix I" with fiber contents of 3.0% and 6.0%.

continuum elements $E_c = 37$ GPa and $\nu = 0.2$; whereas the parameters of the inelastic interface result in $k_N = 1000$ MPa/mm, $k_T = 200$ MPa/mm, $\tan(\phi_0) = \tan(\beta_0) = \tan(\phi_r) = 0.6$, $\chi_0 = 4$ MPa, $c_0 = 7.0$ MPa, $G_f^I = 0.12$ N/mm, $G_f^{IIa} = 10G_f^I$, $\sigma_{dil} = 10$ MPa. The remaining interface parameters are considered equal to zero. Some of the relevant fiber parameters are derived from their main mechanical properties, while the others arise from a calibration procedure, as $E_d = E_s$, $\sigma_{y,d} = 18\%\sigma_{y,s}$, $k_c = 440$ N/mm^3, $\alpha_f = 7.7$ and $H_f = K_f = 0$.

The comparison between model predictions and the experimental data by Li et al. [38] for the uniaxial tensile test in terms of stress-opening cracking diagrams (σ - u) are reported in Fig. 5, regarding SFRC with uniformly distributed Dramix type II steel fibers and fiber contents $\rho_f = 3.0\%$, 3.5% and 4.0% on the left hand side, while the graphics on the right hand side show the model predictions for panels with Dramix type I fibers and fiber contents $\rho_f = 6.0\%$, 7.0% and 8.0%. The numerical predictions for the uniaxial tensile tests demonstrate that the proposed constitutive model reproduces the increment of toughness and strength with increasing fiber content and hence their ductility rise and higher released energy values are obtained.

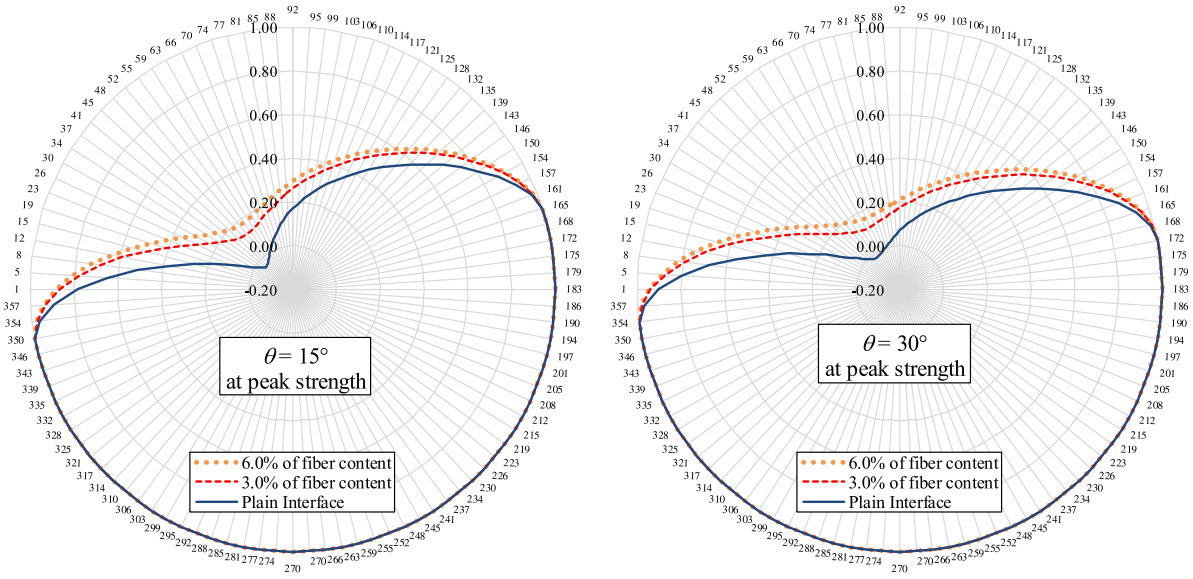

Fig. 12. CI polar plots for $\theta = 15°$ and $\theta = 30°$ (fracture mixed modes with prevalent shear).

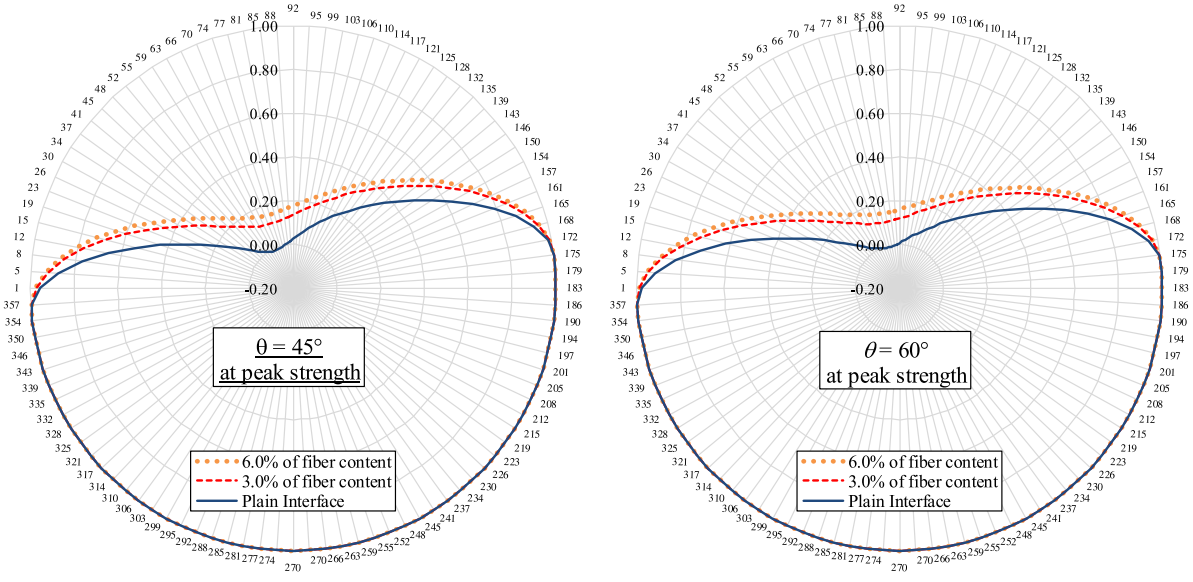

Fig. 13. CI polar plots for $\theta = 45°$ and $\theta = 60°$ fracture mixed modes.

5. Failure performance and cracking indicators

This section is aimed at analyzing the influence of both stress states and steel fiber amounts on the failure modes and post-cracking performance of the SFRC. The numerical results for the dimensionless CI presented in this section are based on the numerical analysis explained in Section 3.2. The CI has been computed for variable fibers qualities and load (fracture) scenarios. Peak stresses are applied on three different SFRC, i.e. plain concrete, Dramix I steel fibers FRCC with 3.0 and 6.0%. All the numerical predictions refer to the model parameters calibrated in Section 4.2.

It is worth remembering that the Cracking Indicator CI for DCA varies as a function of two fundamental angles, i.e. θ defining the stress state (lying upon the loading surface), and ρ indicating all possible directions of the discontinuity surface. The minimum CI value for each ϕ-angle determines the weakness direction of the considered interface/joint.

A set of six interface stress states are selected and analyzed for each SFRC type: (i) Uniaxial tension: $\theta = 90°$ (namely pure mode I); (ii) Tension–shear with prevalence of tensile stress: $\theta = 75°$ and $\theta = 60°$; (iii) Tension–Shear mixed mode I/II of fracture: 45°. (iv) Tension–Shear with prevalence of shear stresses: $\theta = 30°$ and 15°.

The results of these analyses are shown between Figs. 6 to 11, while from Figs. 12 to 14 they are represented via polar plots. Critical values of the ρ_{cr}-angle, representing those stress levels at which CI has reached its minimum, are summarized in Table 4.

As it can be observed, CI assumes negative values only for the analysis cases of plain concretes. This is due to the typical post-cracking softening responses of the zero-thickness interface model, under all cases of fracture in mode I, mode II and mixed cases for plain concrete. Contrarily, positive values of CI are characterizing all the SFRC specimens, with either 3.0% or 6.0% of fiber contents. With these amounts of fibers, the post-cracking behavior of the joint model is characterized by an hardening post-cracking response, consequently all the CIs have values greater than zero. In case of the uniaxial tensile test ($\theta = 90°$), the critical ρ_{cr}-angle (numerically evaluated) is equal to the initial load angle θ for both, plain concrete and all SFRCs. In other words $\rho_{cr} = \theta = 90°$.

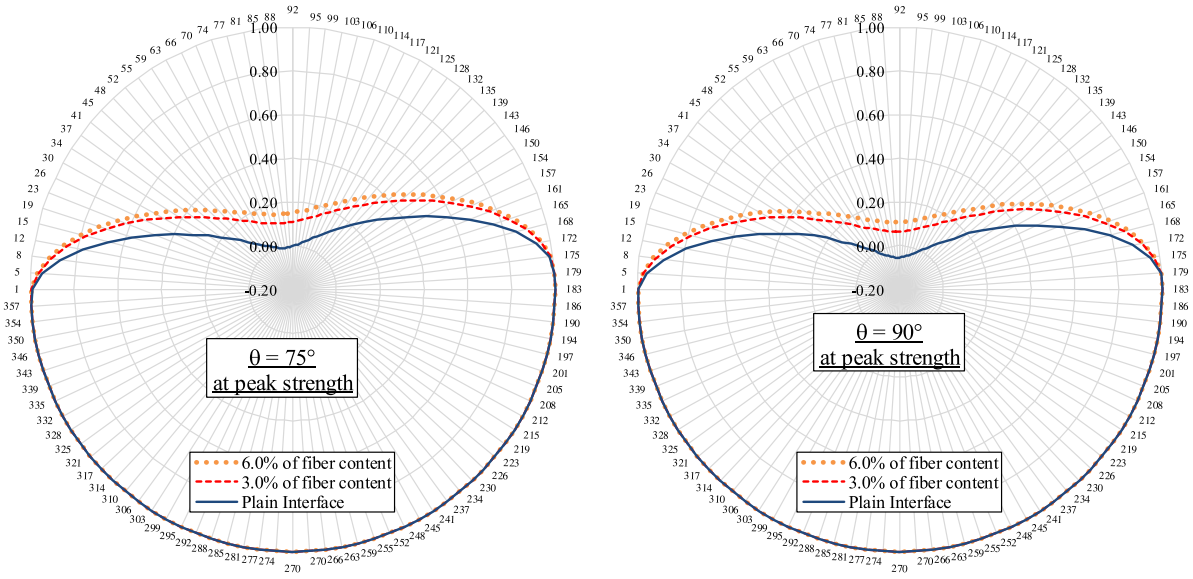

Fig. 14. CI polar plots for fracture mixed modes with prevalent normal failure $\theta = 75°$ and pure mode I $\theta = 90°$.

It is interesting to note that when the analysis of CI is moving from pure mode I towards modes II (i.e. from $\theta = 90°$ towards $\theta = 75°$, $\theta = 60°$, $\theta = 45°$, $\theta = 30°$ and $\theta = 15°$), the ρ_{cr} (indicating the minimum values for CI analysis) assumes a value always lower than the initial loading angle θ: i.e., $\rho_{cr} < \theta$ always in mixed modes I/II. The difference $\theta - \rho_{cr}$ reaches its maximum for the case of mixed fracture with prevalence of shear stresses and the minimum of null value for pure mode I. This is a clear indicator the weakest and "preferred" path for cracking mechanisms for both plain concrete and SFRC is the pure mode I.

The influence of the fiber content is also relevant in all cases. Fiber contents clearly affect both the indicator value and critical failure directions, much more in mixed fracture mechanisms that for the tensile one. The CI values them self are barely influenced. Interesting is the analysis of the difference $\theta - \rho_{cr}$ between plain concrete and SFRC with 3.0% or 6.0% of fiber contents (see Table 4). Looking at the same initial θ value, the difference $\theta - \rho_{cr}$ becomes bigger for SFRC with higher amounts of fiber contents. This is a clear message that the fiber bridging mechanisms clearly enhance the mode I fracture toughness of the SFRC joint (see Fig. 14).

It is worth finally noticing that the proposed DCA failure indicators explicitly incorporate the influence of fibers and the content of them on the failure directions. Unlike the SCA approach for which the failure direction is only determined by the more brittle phase that plasticizes, and only depending on the cementitious matrix, it is not influenced by the fiber content (see Vrech et al. [32]).

6. Concluding remarks

In this work, a fracture-based interface constitutive theory, aimed at predicting the failure behavior of FRCC, has been developed. The formulation is founded on a DCA and considers the well-known Mixture Theory to smear the fibers effects. Bridging interactions of fibers crossing cracks are modeled in the form of fiber-to-concrete bond–slip and dowel mechanisms. In addition, a novel concept was presented for evaluating the most critical direction for further loading by means of a so-called normalized Cracking Indicator (CI) which was formulated in this work for the FRCC interface model. The CI accounts for the mechanical degradation in all different constituents of the mixture and, consequently, allows to evaluate the dependence on the fibers direction and content of the energy release evolution and how these parameters affect the most critical direction for further loading. The numerical analyses demonstrated that the constitutive proposal captures the fundamental features of the FRCC mechanical behavior. Very good agreements between numerical results against experimental data, available in scientific literature, have been achieved in terms of peak-strength and post-cracking toughness for uniaxial tensile and fracture mixed modes tests. Finally, the performance of CI, proposed in this work as an extension of the normalized indicator for diffuse failure by Hill's condition of stability and now suitable for DCA approaches, was demonstrated that can correctly predict the crack onset and the critical directions for further loading in terms of the fiber contents and different fracture scenarios.

Declaration of competing interest

The authors declare the following financial interests/personal relationships which may be considered as potential competing interests: Antonio Caggiano reports a relationship with University of Genoa that includes: employment.

Data availability

Data will be made available on request.

Acknowledgments

The authors would like to express their gratitude for the financial support provided by CONICET, Argentina - PIP 11220170100795CO, the Univ. of Buenos Aires, Argentina - UBACyT 20020190200208BA, and CIUNT - PIUNT E613.

References

[1] S. Wang, H. Zhu, F. Liu, S. Cheng, B. Wang, L. Yang, Effects of steel fibers and concrete strength on flexural toughness of ultra-high performance concrete with coarse aggregate, Case Stud. Constr. Mater. (2022) e01170.

[2] I. Curosu, V. Mechtcherine, O. Millon, Effect of fiber properties and matrix composition on the tensile behavior of strain-hardening cement-based composites (SHCCs) subject to impact loading, Cem. Concr. Res. 82 (2016) 23–35.

[3] A.P. Fantilli, H. Mihashi, P. Vallini, Multiple cracking and strain hardening in fiber-reinforced concrete under uniaxial tension, Cem. Concr. Res. 39 (12) (2009) 1217–1229.

[4] A. Caggiano, M. Cremona, C. Faella, C. Lima, E. Martinelli, Fracture behavior of concrete beams reinforced with mixed long/short steel fibers, Constr. Build. Mater. 37 (2012) 832–840.

[5] L. Facconi, F. Minelli, How can we verify structural members made of FRC only? in: RILEM-Fib Int Symp on FRC, Springer, 2021, pp. 525–535.
[6] M. Xu, K. Wille, Fracture energy of UHP-FRC under direct tensile loading applied at low strain rates, Composites B 80 (2015) 116–125.
[7] Faserbeton-R, Osterreichische Vereinigung fur Beton-und Bautechnik, OBBV, Wien, 2002.
[8] AFGC-SETRA, Ultra High Performance FRC, Interim Recommendations, AFGC Publication, France, 2002.
[9] DBV, Merkblatt "Stahlfaserbeton" (SFRC Leaflet), Deutscher Beton- und Bautechnik-Verein E.V., Germany, 2001.
[10] CNR-DT-204, Guidelines for Design, Construction and Production Control of Fiber Reinforced Concrete Structures, National Research Council of Italy, 2006.
[11] EHE08, Comisión Permanente del Hormigón, Instrucción del Hormigón Estructural, Spanish Code, 2008.
[12] Stalfiberbetong, Rekommendationer for Konstruction, utforande och provning Betongrapport N.4, Svenska Betongforeningen, Betongrapport, 1995.
[13] SIA-162-6, Stahlfaserbeton, Schweizerischer Ingenieur und Architekten-Verein, Postfach, 8039 Zurich, 1999.
[14] RILEM-TC162-TDF, Test and design methods for steel fibre reinforced concrete - σ - ϵ design method: final recommendation, Mater. Struct. 36 (262) (2003) 560–567.
[15] fib-Model-Code, Model Code 2010 - First Complete Draft, vol. 1, Comité Euro-International du Beton-Federation International de la Precontrainte, Paris, 2010.
[16] ACI-544.4R-88, Design Considerations for Steel Fiber Reinforced Concrete, ACI Farmington Hills, 1996.
[17] ACI-318-08/318R-08, ACI Committee 318, Building Code and Commentary, ACI Farmington Hills, 2008.
[18] J. Bi, L. Huo, Y. Zhao, H. Qiao, Modified the smeared crack constitutive model of fiber reinforced concrete under uniaxial loading, Constr. Build. Mater. 250 (2020) 118916.
[19] B. Yin, L. Zhang, Phase field method for simulating the brittle fracture of fiber reinforced composites, Eng. Frac. Mech. 211 (2019) 321–340.
[20] X. Li, W. Gao, W. Liu, A mesh objective continuum damage model for quasi-brittle crack modelling and finite element implementation, Int. J. Damage Mech. 28 (9) (2019) 1299–1322.
[21] M. Cervera, J. Wu, On the conformity of strong, regularized, embedded and smeared discontinuity approaches for the modeling of localized failure in solids, Int. J. Solids Struct. 71 (2015) 19–38.
[22] A. Wosatko, A. Genikomsou, J. Pamin, M.A. Polak, A. Winnicki, Examination of two regularized damage-plasticity models for concrete with regard to crack closing, Eng. Fract. Mech. 194 (2018) 190–211.
[23] A. Caggiano, G. Etse, E. Martinelli, Zero-thickness interface model formulation for failure behavior of fiber-reinforced cementitious composites, Comput. Struct. 98 (2012) 23–32.
[24] C. Del Prete, I. Boumakis, R. Wan-Wendner, J. Vorel, N. Buratti, C. Mazzotti, A lattice discrete particle model to simulate the viscoelastic behaviour of macro–synthetic fibre reinforced concrete, Constr. Build. Mater. 295 (2021) 123630.
[25] M.F. Benedetto, A. Caggiano, G. Etse, Applications of the virtual element method for cracking analysis of cement-based composites using interface elements, Mec. Comput. 34 (37) (2016) 2555–2566.
[26] T. Rukavina, A. Ibrahimbegovic, I. Kozar, Multi-scale representation of plastic deformation in fiber-reinforced materials: application to reinforced concrete, Lat. Am. J. Solids Struct. 16 (2019).
[27] J. Oliver, A.E. Huespe, P.J. Sánchez, A comparative study on finite elements for capturing strong discontinuities: E-FEM vs X-FEM, Comput. Methods Appl. Mech. Engrg. 195 (37–40) (2006) 4732–4752.
[28] N.S. Ottosen, K. Runesson, Properties of discontinuous bifurcation solutions in elasto-plasticity, Int. J. Solids Struct. 27 (4) (1991) 401–421.
[29] J. Hadamard, Leçons sur la Propagation des Ondes et Les Équations de L'Hydrodynamique, A. Hermann, 1903.
[30] T.Y. Thomas, Plastic Flow and Fracture in Solids By Tracy Y Thomas, Elsevier, 1961.
[31] R. Hill, Acceleration waves in solids, J. Mech. Phys. Solids 10 (1) (1962) 1–16.
[32] S. Vrech, G. Etse, A. Caggiano, Thermodynamically consistent elasto-plastic microplane formulation for fiber reinforced concrete, Int. J. Solids Struct. 81 (2016) 337–349.
[33] I. Carol, P. Prat, C. Lopez, Normal/shear cracking model: Applications to discrete crack analysis, J. Engrg. Mech. - ASCE 123 (1997) 765–773.
[34] G. Etse, A. Caggiano, S. Vrech, Multiscale failure analysis of fiber reinforced concrete based on a discrete crack model, Int. J. Fract. 178 (1) (2012) 131–146.
[35] A. Caggiano, E. Martinelli, A unified formulation for simulating the bond behaviour of fibres in cementitious materials, Mater. Des. 42 (2012) 204–213.
[36] G. Etse, K. Willam, A fracture energy-based constitutive formulation for inelastic behavior of plain concrete, ASCE-JEM 120 (1994) 1983–2011.
[37] M. Hassanzadeh, Determination of fracture zone properties in mixed mode I and II, Eng. Frac. Mech. 35 (4–5) (1990) 845–853.
[38] F. Li, Z. Li, Continuum damage mechanics based modeling of FRC in tension, Int. J. Solids Struct. 38 (5) (2001) 777–793.